Paper:
Verdon, JP, Kendall, JM, White, DJ and Angus, DA (2011) *Linking microseismic event observations with geomechanical models to minimise the risks of storing CO2 in geological formations.* Earth and Planetary Science Letters, 305 (1-2). 143 - 152. ISSN 0012-821X

http://dx.doi.org/10.1016/j.epsl.2011.02.048

Linking microseismic event observations with geomechanical models to minimise the risks of storing CO_2 in geological formations

J.P. Verdon[a,*], J-M. Kendall[a], D.J. White[b], D.A. Angus[c]

[a] *Department of Earth Sciences, Wills Memorial Building, University of Bristol, Bristol, U.K..*
[b] *Geological Survey of Canada, 580 Booth, Ottawa, Canada.*
[c] *School of Earth & Environment, University of Leeds, Leeds, U.K..*

Abstract

For carbon capture and storage (CCS) in geological formations to be scientifically viable, we must be able to model and monitor the effects of geomechanical deformation on the integrity of the caprock. Excess deformation may open fractures, providing pathways for CO_2 leakage from the reservoir. An acceptable geomechanical model must provide a good match with field observations. Microseismic activity is a direct manifestation of mechanical deformation, so can be used to constrain geomechanical models. The aim of this paper is to develop the concept of using observations of microseismic activity to help groundtruth geomechanical models. Microseismic monitoring has been ongoing at the Weyburn CO_2 Storage and Monitoring Project since 2003. We begin this paper by presenting these microseismic observations. Less than 100 events have been recorded, documenting a low rate of seismicity. Most of the events are located close to nearby producing wells rather than the injection well, a pattern that is difficult to interpret within the

*Corresponding author
Email addresses: James.Verdon@bristol.ac.uk (J.P. Verdon), gljmk@bristol.ac.uk (J-M. Kendall), Don.White@NRCan-RNCan.gc.ca (D.J. White), D.Angus@leeds.ac.uk (D.A. Angus)

Preprint submitted to EPSL *January 18, 2011*

conventional framework for injection-induced seismicity. Many events are located in the overburden. Without geomechanical simulation it is difficult to assess what these observations mean for the integrity of the storage formation. To address these uncertainties we generate numerical geomechanical models to simulate the changes in stress induced by CO_2 injection, and use these models to predict the generation of microseismic events and seismic anisotropy. The initial geomechanical model that we generate, using material properties based on laboratory core measurements, does not provide a good match with either event locations or S-wave splitting measurements made on the microseismic events. We find that an alternative model whose reservoir is an order of magnitude softer than lab core-sample measurements provides a much better match with observation, as it leads shear stresses to increase above the production wells, promoting microseismicity in these areas, and generates changes in effective horizontal stresses that match well with S-wave splitting observations. This agreement between geophysical observations and a softer-than-lab-measurements reservoir model highlights the difficulties encountered in upscaling lab scale results. There is a strong need to link geomechanical models with observable manifestations of deformation in the field, such as induced seismicity, for calibration. Only then can we accurately assess the risks of leakage generated by mechanical deformation.
Keywords: Geological carbon storage, Weyburn, Carbon dioxide, Passive seismic monitoring, Geomechanical modelling

1. Introduction

Storage of CO_2 in deep geological formations such as saline aquifers and mature hydrocarbon reservoirs provides a technique that can immediately reduce mankind's greenhouse gas emissions while continuing to meet the world's energy needs. As we consider the development of large scale storage sites – the EU has proposed that at least 12 CCS sites should be in operation by 2015 – it is clear that monitoring programs will be required to demonstrate that CO_2 is safely stored, and also that effective modelling tools should be developed to predict the fate of injected CO_2 (Bickle et al., 2007). It is necessary not just to model the flow of CO_2 through the subsurface, but also the mechanical deformation that CO_2 injection can induce. There are a host of uncertainties that beset the accurate modelling of subsurface processes, which means that models can only be trusted when they provide a good match with observations made at the site. This is why Directive 2009/31/EC of the European Parliament, on geological storage of CO_2, states that 'the minimum conditions for site closure and transfer of responsibility includes [...] the conformity of the *actual* behaviour of the injected CO_2 with the *modelled* behaviour' (E.U. Parliament and Council, 2009). For reservoir flow modelling, the accuracy of a model is confirmed by history matching with known wellhead pressures, CO_2 breakthrough at observation wells (Giese et al., 2009), and matching the plume shape with that inferred from 4D seismic monitoring (Arts et al., 2004; Bickle et al., 2007).

Injection of CO_2 will increase the pore pressure in the reservoir, deforming both the reservoir and sealing caprocks. Excess deformation can compromise caprock integrity through the formation or reactivation of fractures or faults. It is therefore important to model the geomechanical impact of CO_2 injection. Geomechanical models can also be used to ensure that CO_2 injection does not induce earthquakes on nearby faults. Just as fluid flow models are matched with observations, so we must do so with geomechanical models to ensure that they are accurately representing reality. There are several techniques that can be used to constrain geomechanical models, such as surface deformation, 4D seismic observations and microseismic activity. At In Salah, Algeria, CO_2 injection has produced surface deformation, which has been imaged using satellite based InSAR methods (Onuma and Ohkawa, 2009). The magnitude and geometry of the surface deformation provides a constraint to guide geomechanical models (Rutqvist et al., 2009). Increases in P-wave travel time detected during 4D seismic surveys have been used to image deformation in the overburdens of depleting reservoirs (Hatchell and Bourne, 2005). However, this technique has yet to be applied to a CO_2 storage site, where, presumably, the expansion of the reservoir would compress the overburden, reducing P-wave travel times (e.g., Verdon et al., 2008b).

In this paper we will demonstrate how microseismic activity can be used to constrain geomechanical models. Movement of faults and/or fractures will generate seismic energy. Although analogous to earthquakes, event magnitudes in and around reservoirs are significantly lower, so they are termed *microearthquakes* or *microseismic events*. The seismic waves that are produced by such events can be detected by geophones placed in boreholes, or larger arrays at the surface. Events are located using methods derived from conventional earthquake seismology. Given that microseismic events will be induced by stress and pressure changes caused by CO_2 injection, they represent an observable manifestation of geomechanical deformation that can be used to constrain mechanical models.

Seismic waves generated by microseismic events and recorded on geophones near the reservoir will travel through the rocks that are directly of interest (as opposed to controlled source seismics, where waves must travel through the whole of the overburden to and from the surface). As such, wave propagation effects can also provide information about geomechanical processes. Of particular interest is seismic anisotropy, where the velocities of waves are dependent on their direction of travel and polarisation.

It is well known that seismic velocities and anisotropy are modulated by non-hydrostatic stress changes (e.g., Nur and Simmons, 1969; Zatsepin and Crampin, 1997; Teanby et al., 2004b; Verdon et al., 2008a), so observations of shear wave splitting – a key indicator of anisotropy – made on waves generated by microseismic events can also be used to inform geomechanical models.

1.1. The Weyburn CO_2 Monitoring and Storage Project

The Weyburn field in Saskatchewan, Canada, has been producing oil since 1954. Waterflooding was initiated in the 1960s to maintain production levels, and horizontal infill wells were drilled in the 1990s. Injection of CO_2 began in 2000, which boosted oil production back to 1970s levels. Approximately 3 million tonnes of CO_2 are injected each year in a supercritical state. The CO_2 injection program has included a research component, testing and examining the abilities of various monitoring techniques to image CO_2 in the subsurface. The results of this research are of great significance for the CCS community.

The Weyburn reservoir, at a depth of ~1430m, consists of an upper Marly dolostone and lower Vuggy limestone layer, of Carboniferous age, with a combined thickness of 30-40m. The reservoir is over- and underlain by thin evaporite layers, which provide the primary seal, while a secondary seal is provided by the overlying Mesozoic Watrous shale layer. Controlled source seismic monitoring combined with reservoir fluid flow modelling has been successful in imaging the plumes of CO_2 migrating away from the injection wells (White, 2009). In 2003 it was decided to examine the feasibility of using microseismic monitoring to image the injection of CO_2 in one pattern of the field. Weyburn is the first – and currently the largest – CCS site to have deployed a microseismic event detection array. Microseismic arrays have also been installed at the Aneth oil field CCS-EOR pilot site, Utah (Zhou et al., 2010), and recently at the In Salah CCS site, Algeria (Mathieson et al., 2010).

A recording array of 8 triaxial geophones was cemented in a disused vertical production well approximately 50m from a vertical CO_2 injection well. Horizontal production wells trending to the NE are located to the NW and SE of the injection well. The setup for microseismic monitoring can be seen in Figure 1. The geophones were spaced at 25m intervals at depths between 1181-1356m. The geophones were switched on in August 2003, and CO_2 injection began in January 2004. Excepting two short periods where the array was shut down for technical reasons, recording has been continuous until the present. The passive seismic experiment is divided into two phases – Phase IB which began in August 2004 and ran until October 2004, and Phase II, which has run from September 2005 until 2010.

2. Observed microseismicity

Further information on the microseismicity observed at Weyburn can be found in Maxwell et al. (2004), White (2009) and Verdon et al. (2010b). To locate detected seismic triggers, a 1D P- and S-wave velocity model was computed using a dipole sonic velocity log from a nearby well. Locations were calculated by matching observed P- and S-wave arrival times with ray-tracing through the model, and the propagation azimuth was determined using first arrival P-wave hodogram analysis.

Event locations are marked in Figure 1. 68 triggers were detected during Phase IB that were from microseismic events (rather than completion shots or drilling noise) and could be reliably located. This represents a very low rate of seismicity. Events have magnitudes of -1 to -3, and events of magnitude -2 are detectable at 500m from the array, which suggests that the small number of events recorded is not an artifact of high noise levels.

During Phase II, 18 events were detected in October 2005, and 21 in January 2006. As of 2006 no further events have been detected. There is no evidence to suggest that increases in reservoir noise, or equipment failure, are to blame for the lack of seismicity post 2006, as other activities such as drilling and well completions continue to be detected. The lack of seismicity post 2006 means that CO_2 is moving through the reservoir aseismically. This may indicate that either little deformation is occurring, or that deformation is occurring in a more ductile manner, such that microseismic events are not generated. Verdon et al. (2010a) have shown that CO_2 injection can generate similar amounts of of seismicity to water injection, so it is unlikely that it is the lower bulk modulus and/or viscosity of CO_2 alone that has generated the low seismicity rates.

There is a range of dominant frequencies in the events detected, from as low as 20Hz to 150Hz (Verdon et al., 2010b). Because the recording environment at Weyburn is relatively noisy, and because many events have low (20Hz) dominant frequencies, errors in event location are often large (up to 100m in depth). Furthermore, perturbations to the velocity model of $\pm 250 \mathrm{ms}^{-1}$ can change event locations by 75m N-S, 20m E-W and 70m vertically. Nevertheless, these relatively large location uncertainties do not affect our principal conclusions.

The hypocenters plotted in Figure 1 show that most of the events are located near to the production wells to the NW and SE. Conventional wisdom dictates that as pore pressures increase around the injection well, effective normal stress will decrease, moving the stress state (often plotted in Mohr circle notation) closer to the Mohr-Coulomb failure criteria. As a result, microseismic events will initially be located around the injection site, and will move outwards radially to track the pressure pulse (e.g., Shapiro, 2008, and references therein). At production wells, the pressure drawdown will increase the effective normal stress, reducing the likelihood of shear failure. Therefore the observations made here, with events located near producing wells, and few events at the injector, were not expected.

Many events appear to be located above the reservoir. Although the large depth errors mean that some of these events could actually be located within the reservoir interval, it seems that much of the microseismic activity is occurring in the overburden. Does this indicate top-seal failure and the migration of CO_2 into the overburden? Stress arching effects – where part of the load induced by CO_2 injection is taken up by stress transfer into the over-, under- and sideburdens – can also lead to seismicity in the overburden (e.g., Angus et al., 2010), without any transfer of fluid or of pore pressure between the reservoir and caprocks. This underscores the importance of having a good understanding of the potential geomechanical behaviour of the storage site in different hypothetical circumstances. It is probable that fluid migration or a pore-pressure connection into the overburden will be documented by a different spatial and temporal pattern of microseismicity compared to stress arching effects – geomechanical models will be necessary to distinguish them.

2.1. Anisotropy

The seismic energy recorded on the geophones will have travelled only through rocks in and near the reservoir. As such, wave propagation effects such as S-wave splitting (SWS) induced by seismic anisotropy can be attributed to the physical properties of these rocks. This means that microseismic events make ideal shear-wave sources for SWS analysis (Verdon and Kendall, 2011), because there is no need to account for the anisotropy of all the rock between the surface and the reservoir interval, as with SWS measured using 9-component reflection seismic surveys (e.g., Luo et al., 2005, 2007). In hydrocarbon reservoirs, anisotropy is usually caused by the presence of aligned fracture sets. By forward modelling the effects of fractures and sedimentary fabrics, it is possible to invert measurements of SWS for combinations of fracture geometries that best fit the observed data (Verdon et al., 2009). The SWS detected by the geophones was measured using the semi-automated technique developed by Teanby et al. (2004a), using cluster analysis to ensure a stable result.

Of the 544 possible SWS measurements during Phase IB, (68 events × 8 geophones) only 30 provided reliable results, quite a low success rate for SWS analysis. This is partly related to the fact that the low frequency of the waveforms causes the S-wave arrivals to be contaminated by P-wave coda, and partly related to the fact that the S:N ratio of the waveforms is not very good. The measurements are plotted in Figure 2a. The measurements are inverted for the strikes and fracture densities of two vertical fracture sets – this approximates the observations made on core samples regarding aligned fractures in the reservoir (Brown, 2002). Fracture density refers to the nondimensional term given by Hudson et al. (1996). To visualise the results of the inversion we plot the normalised rms misfit between forward modelled and observed splitting as a function of the two fracture strikes and densities (Figure 2b & 2c). The 90% confidence intervals are marked in bold – the inversion finds well constrained fracture strikes of 150° and 42°. The fracture densities are less well constrained because they trade off against each other, but all successful inversion results imply that the fracture set at 150° (F1) has a higher fracture density than the set at 42° (F2).

The observed splitting is a path averaged effect, which includes contributions from all the portions of the rock through which the waves have travelled. The waves from some of the events, which are located in the reservoir, will have travelled through both reservoir and overburden rocks, while waves from events in the overburden will have travelled through the overburden only. As such, the observed splitting will contain contributions from both the overburden and reservoir, and it will be difficult to decompose these effects. Previous work on the reservoir interval has indicated the presence of fractures sets striking at 40°and 148°(Brown, 2002), matching closely the fracture sets inferred from SWS observations. No such data is available for the overburden. However, Brown (2002) found that the NE striking set (F2 here) is the more pervasive set, while the SE set (F1 here) is weaker. This contrasts with the inversion of SWS observations, which suggest that the F1 set is the more dominant.

The above indicates that the observations made during microseismic monitoring do not provide a wholly satisfactory match with expectations. The event hypocenters are generally located around the horizontal production wells, and some appear to be in the overburden, rather than around the injection well as expected. These locations cannot be explained without resorting to some form of geomechanical modelling, and it is important to determine whether the seismicity in the overburden represents fluid migration or merely stress transfer. Seismic anisotropy is also sensitive to non-hydrostatic stress changes, so such geomechanical models may also help understand why the observations of seismic anisotropy do not fully match the observations made on boreholes and core samples made by Brown (2002). In the following section we develop a simple geomechanical model to represent the deformation caused by injection into the Weyburn reservoir.

3. Geomechanical modelling

While widely used for civil engineering applications, finite element mechanical modelling is still a developing technique in the earth sciences. The state of the art is to couple together an industry-standard reservoir flow simulator with a finite element mechanical solver (Dean et al., 2003). The reservoir flow simulation provides the pore fluid pressures, fluid densities and compressibilities, which are used as the loading for the geomechanical simulations.

There are a number of methods with which to couple together the flow and mechanical simulators (Dean et al., 2003). The simplest is with a one-way coupling, where the results from the flow simulation at user-defined timesteps are used as the loading for a geomechanical model, with no feedback to the flow simulator from the geomechanical results. This approach is appropriate where the deformation is slight enough that it does not cause significant variation in porosity and/or permeability. Where deformation is large enough to moderate the flow properties, changes in porosity and permeability must be returned to update the fluid flow simulation.

The most effective balance between numerical accuracy, computational time, and the functionality provided by industry-standard software, is found in an iterative method, where the fluid flow simulation and geomechanical model are solved iteratively until a convergent value for the change in pore volume is found for each timestep (Dean et al., 2003). This is the method we use to model the CO_2 injection at Weyburn, coupling together a MORE (by Roxar Ltd) fluid flow simulation with an ELFEN (Rockfield Ltd) geomechanical model via a Message Passing Interface (MPI, also by Rockfield Ltd).

3.1. Fluid flow simulation

The fluid flow simulation only has to simulate the reservoir. Because the reservoir is laterally extensive with little topography, it is appropriate to model it as a flat layer with a structured mesh. We set up the injection and production wells to approximate the pattern at Weyburn where microseismic monitoring has been deployed. 4 horizontal wells are modelled, trending parallel to the y axis. In between the production wells are 3 vertical injection wells with a spacing in the y direction of 500m. The horizontal wells are completed over a length of 1400m in the reservoir. To reduce computational requirements we model only half of the reservoir, and complete the simulation by assuming that the model is symmetrical about the x axis. Therefore the figures in this work show only the half of the reservoir that has been simulated.

The region enclosed by the wells is approximately 1.5×1.5km. However, we extend the model to 4.4km in the x direction and 4km in the y direction in order to avoid the influence of edge effects. The reservoir is 40m thick, and for the purpose of fluid flow simulation is split into the upper Marly and lower Vuggy layers. The modelled porosities are 0.25 for the Marly layer and 0.15 for the Vuggy layer, and the permeabilities are κ_x=5mD, κ_z=4mD for the Marly layer, and κ_x=10mD, κ_z=7mD for the Vuggy layer. These values are chosen as representative of geological models of the reservoir, which show heterogeneity typical of carbonate systems. Nevertheless, these values provide a reasonable match with observed pressures and injection rates, although the simulation has not been history matched in any way.

The mesh through the well region has a spacing of 60×50m ($x \times y$), with an increasingly coarse mesh used away from the wells. The flow regime is as follows: For one year there is no injection in order to ensure that the model has stabilised; after this the field is produced, representing the pressure drawdown during oil production at Weyburn, reducing the pore pressures from 15 to 10MPa. The three vertical wells then begin to inject CO_2, for a period of 1 year, increasing the pressure to ∼18MPa, while the pressure is still below 15MPa at the producers. This provides an approximation of the state of the field after 1 year of injection (i.e., by the end of 2004, the end of Phase IB). The CO_2 injection rate at each well is 100MSCM/day. The pore pressures, which provide the loading for the geomechanical model, at the end of the simulation are plotted in Figure 3.

3.2. Geomechanical model

The geomechanical model must include both the reservoir and the surrounding over- and underburden. The geometry of the reservoir in the geomechanical model must be the same as for the fluid flow modelling. However, the internal mesh need not be the same, as we are able to interpolate between the simulators. For the geomechanics we use a mesh spacing of 60×50×20m ($x \times y \times z$) in the reservoir, coarsening away from the wells. The top of the reservoir is at 1430m. The overburden is modelled to the surface. As with the reservoir, the units in the overburden are assumed to be flat and laterally continuous layers, modelled with a regular grid. The underburden is modelled to a depth of 2480m, 1km below the base of the reservoir. The non pay rocks are divided into 4 units: the evaporite units bounding the reservoir both above and below, the overlying Watrous shale, while the remainder of the overburden above the Watrous, and the underburden below the lower evaporite layers are modelled with uniform representative properties. The properties of these layers further from the reservoir do not significantly affect the stress evolution in and around the reservoir with which we are concerned, so treating them in this manner is not an issue.

The geomechanical model is solved for a poroelastic regime, where deformation is dependent on the Young's modulus (E), Poisson's ratio (ν) and porosity (ϕ) of the rocks, as well as the compressibility of the pore fluid, which is assumed to be brine in all of the non-pay rocks. The material properties for each unit are given in Table 1, based on core sample work by Jimenez et al. (2004). The boundary conditions are that the top of the model is a free surface, and the planes at the sides and base of the model are prevented from moving in a direction normal to the boundary, although they are free to move within the plane of the boundary (i.e. at the $x - z$ boundary, nodes can move vertically (z), and horizontally in the x direction, but not in the y direction).

4. Results

During the production phase of the simulation, the pore pressure drawdown increases the effective stress in the reservoir, while there is a small amount of extension in the overburden. During the injection phase, the effective stress decreases at the injection well as the pore pressure increases. The inflation of the reservoir causes a small amount of compaction in the overburden. Plots of the changes in effective stress in and around the reservoir can be found in the online supplementary material. The stress changes in the overburden are small, most of the load induced by injection is taken up by the reservoir. We are most interested in what these stress changes mean for induced seismicity, as this will allow us to compare our model to the microseismic observations made at Weyburn. Therefore we develop a method to map modelled stress changes into predictions about the likelihood of generating induced seismicity.

4.0.1. Induced Seismicity

We have not modelled discrete surfaces on which failure may occur. The area of rock stimulated by a microseismic event is typically on a sub-metre scale, whereas the elements we use in geomechanical modelling have dimensions of ∼50m. Therefore, in order to generate predictions about microseismic event locations we need a way of approximating the likelihood of a microseismic event occurring in a particular model element. To do so we use the concept of the fracture potential, as described in Eckert (2007).

The likelihood of a material to experience brittle shear failure can be expressed in terms of a fracture potential, f^p (Connolly and Cosgrove, 1999).

The fracture potential describes how close the stress state is to crossing the Mohr-Coulomb envelope described by

$$\tau = m\sigma'_n + c, \tag{1}$$

where τ is the shear stress and σ'_n is the effective normal stress acting on the rock, and m is the coefficient of friction and c is the cohesion of a plane in the rock. m is often given in terms of an angle of friction,

$$m = \tan \phi_f. \tag{2}$$

The shear stress, τ is related to the differential stress, q, which is the difference between maximum and minimum effective stress, by

$$\tau = q/2 = \frac{\sigma'_1 - \sigma'_3}{2}. \tag{3}$$

In the shear failure regime, f^p describes the ratio between the actual differential stress and the critical differential stress at failure,

$$f^p = \frac{q}{q_{crit}}. \tag{4}$$

The critical differential stress is given by

$$q_{crit} = 2\left(c\cos\phi_f + p\sin\phi_f\right), \tag{5}$$

where p is the mean principal effective stress,

$$p = (\sigma'_1 + \sigma'_2 + \sigma'_3)/3. \tag{6}$$

By substituting equation 5 into equation 4, the fracture potential is then given by

$$f^p = \frac{q}{2(c\cos\phi_f + p\sin\phi_f)}. \tag{7}$$

To compute the fracture potential we use equation 7. In the caprock, we use c=5MPa, ϕ_f=45°, while in the reservoir we use c=3.5MPa, ϕ_f=40°. Because little can be known about preexisting planes of weakness on which brittle shear failure, and therefore microseismicity, will occur, these are rather arbitrary, generic values. However, we are only interested in relative changes in f^p, i.e. whether injection causes f^p to rise or to drop, increasing or decreasing the likelihood of shear failure and microseismic activity. As such, sensitivity analysis shows that the choice of value for these parameters is not particularly important.

In Figure 4 we plot the evolution of fracture potential through time at selected points in the reservoir and overburden. From Figure 4 we note that fracture potential increases in the reservoir during production, while it is relatively unchanged in the overburden. Once injection begins, fracture potential remains relatively constant at the production wells, but decreases at the injection wells. In the overburden there is an increase in fracture potential, albeit limited in spatial extent, above the injection well, with little evolution of f^p elsewhere in the overburden. In Figures 5a and 5b we plot maps of the fracture potential in the reservoir and overburden after 1 year of injection.

In general, there are some qualitative comparisons that can be made between this model and the observations made at Weyburn. For instance, the fact that across most of the reservoir fracture potential is not increased by injection matches with the lack of seismicity recorded. Also, this model suggests that fracture potential should be higher at the production wells than at the injection wells, which matches the observations that the majority of events occur close to the producers. However, this model can not explain why in reality many events are located in the overburden above the producing wells – the model suggests that there is little evolution of f^p in the overburden, and the only place it does increase is directly above the injection well. The suitability of this model can also be assessed through a comparison of the seismic anisotropy that it predicts.

4.0.2. Seismic Properties

To compute the seismic properties based on the stress changes we use the rock physics model developed by Verdon et al. (2008a) and calibrated by Angus et al. (2009). Non-hydrostatic stress changes serve to generate anisotropy by preferential closing of cracks perpendicular to the maximum stress direction, while cracks perpendicular to the minimum stress stay open. Because the majority of the raypaths for the detected S-wave arrivals are through the overburden, we are most interested in the anisotropy generated in this region. The shear-wave splitting patterns generated in the overburden of this model are plotted in Figure 5c. Splitting patterns generated in the reservoir can be found in the online supplementary material. No significant splitting patterns develop in the overburden. Some splitting does develop in the reservoir (see supplementary material), but with a fast direction parallel to the horizontal well trajectories. The lack of anisotropy in the overburden, and anisotropy with fast direction parallel to wells in the reservoir, does not match with the observations made above, where an anisotropic fabric was observed in the overburden, striking to the NW, perpendicular to the horizontal well trajectories.

We conclude that this initial model, whose material properties were based on core measurements from the field, does not provide a good match with the observations of microseismic activity and seismic anisotropy in the field. The question to ask, then, is why this should be? One potential answer lies in the fact that rock physics measurements on cores represent the intact rock, whereas the reservoir is dominated by fractures, which provide key fluid-flow pathways in the reservoir, and, as the name – the Vuggy Formation – suggests, vugs. Core scale measurements can only account for microscale properties – features that are much smaller than the core size. The effects of meso and macro scale features, that are a similar size as, or, in the case of fractures, larger than the cores will not be accounted for in core analysis. The presence of fractures and vugs can significantly soften the elastic stiffness of the reservoir. Because the overburden has far fewer fractures, and no vugs, we keep their properties the same while reducing the stiffness of the reservoir.

4.1. A softer reservoir?

For the updated model, we reduce the Young's modulus of the reservoir to 0.5GPa, while keeping all the other properties the same as for the first model. The trends of effective stress evolution during injection are similar as for the previous model, with increasing pore pressure reducing effective stress at the injection site, and inflation of the reservoir causing compaction in the overburden. However, because in this case the reservoir is softer, more stress can be transferred from the reservoir to the overburden. As a result, the changes in effective stress within the reservoir are reduced, while stress changes in the overburden are amplified. Plots of the effective stress changes in the softer model can be found in the online supplementary material.

The fracture potentials for the softer model are computed as for the first model, using the same Mohr-Coulomb failure criteria. The evolution of f^p through time at selected points in the reservoir is shown in Figure 6. As with the stiffer reservoir, the fracture potential increases during the production phase. As more stress is transferred to the overburden, fracture potential also increases here. Once injection begins, the fracture potential in the reservoir is reduced at the injection well, and remains relatively unchanged at the producing wells. In the overburden above the injection well, after a transient increase in f^p, the fracture potential is reduced in this region, returning to pre-production values. In contrast, the fracture potential in the overburden above the production wells sees an increase after injection, and this increase is maintained throughout the injection period. In Figures 7a and 7b we plot maps of the fracture potential in the reservoir and overburden after 1 year of injection, and the increase in f^p in the overburden above the producing wells is clear.

The evolution of fracture potential for the softer model implies that injection now increases the probability of fracturing in the overburden above the *production* wells, and reduces the probability of fracturing around and above the injection well. This provides a much better match with observations made at Weyburn, where events occur in the reservoir and overburden near the horizontal production wells, but few if any events are found near the injection well. In particular, this model shows how stress transfer into the overburden which, as noted by Segura et al. (2010) is promoted by a softer reservoir, can generate increases in shear stress, and therefore a greater likelihood of microseismicity, above the horizontal production wells.

The shear wave splitting patterns generated in the overburden of the softer model are plotted in Figure 7c. The splitting patterns in the reservoir are available in the online supplementary material. Little splitting is developed in the reservoir. However, in the overburden a coherent splitting pattern develops where the fast directions are orientated parallel to the well trajectories above the production wells (the y axis), while above the injection wells the fast directions are orientated perpendicular to this (parallel to the x axis).

From the recorded data we observed an anisotropic fabric with a fast direction striking to the NW, perpendicular to the NE well trajectories. This splitting was measured on waves recorded by geophones sited between depths of 1181-1356m alongside the injection well, from microseismic events located in or above the reservoir. Therefore, with most of the raypath is in the overburden, the splitting they experience will image the anisotropy of the rocks between event locations and the geophones, i.e., of the caprocks above the injection site. As such, the predictions from the model, with fast directions orientated perpendicular to the well trajectories above the injection well, provide a good match with observations made in Section 2.1, where the dominant fabric was observed striking to the NW, perpendicular to the NE well trajectories.

It appears, therefore, that the model with a reservoir that is an order of magnitude softer than laboratory rock physics measurements produces event location and seismic anisotropy predictions that provide a much better match with observations than the original model. This model implies that the microseismicity observed in the overburden at Weyburn is caused by stress transfer through the rock frame, rather than a pore fluid connection or CO_2 leakage.

5. Discussion

Event locations at Weyburn suggest that there is microseismicity in the overburden. This observation could be a cause for concern, as it could be inferred that the events represent either CO_2 leakage, or at least elevated pore-pressures being transferred into the overburden. Either would imply that pathways exist for CO_2 to migrate out of the reservoir. Nevertheless, controlled source 4-D seismic monitoring has not shown any evidence for fluid migration into the overburden. However, without geomechanical models, there can be no alternative explanation for why the events are found where they are.

A representative geomechanical model shows that, if the reservoir is softer than measured in core samples, deviatoric stress will increase in the overburden, increasing the likelihood of shear failure and thereby of microseismic activity, especially above the producing wells. In contrast, if there were pore-pressure connections, or buoyant fluid leaking into the overburden, one might anticipate that microseismicity would be located above the injection well, where pore pressures are highest and most of the buoyant CO_2 is situated. This has been observed during hydraulic fracturing where CO_2 was used as the injected fluid (Verdon et al., 2010a). At Weyburn events are located above the producing wells, suggesting that the former is the case – a softer than anticipated reservoir is transferring stress into the overburden, inducing microseismicity. The anisotropy generated by such stress transfer also matches the observations of anisotropy made at Weyburn, furthering our confidence in this second, softer model.

It is therefore worth asking whether we are putting the hydraulic integrity of the caprock at risk with these microearthquakes? Unfortunately this question is difficult to answer, as even active faults and fractures do not necessarily act as conduits for fluid flow, and there is no way of knowing how well connected any fractures in the caprock may be. The fact that there are few events, most of which are of low magnitude, suggests that there are not many large scale fractures in the overburden. Furthermore, there has been no seismicity detected more than 200m above the reservoir (Figure 1b), which would be well within the detectability threshold of the geophone array, implying that if any fractures are being stimulated by CO_2 injection, they do not extend far into the caprock system. Most importantly, the suite of integrated geophysical and geochemical monitoring systems deployed at Weyburn do not indicate any leakage, so it would appear that any fracturing generated by microseismicity in the overburden is not currently providing a pathway for leakage. By continuing to monitor the field it will be possible to ensure that this remains the case.

The reduction in stiffness we use to produce the match with observations is large – from 14 to 0.5GPa. This is done to show the changes that a softer reservoir can produce *in extremis*. In this case the changes to fracture potential and shear wave splitting introduced by a softer reservoir are clear for the reader to see. As the stiffness is reduced from 14GPa, the trends that we have highlighted gradually establish themselves. It is well known that the presence of fractures and vugs in a reservoir will mean that core sample measurements are overestimates of the true, *in situ* values. However, an order of magnitude overestimate is perhaps too much to attribute entirely to the presence of fractures and vugs. It is at this point that we should remind ourselves that what we are dealing with here is a simplified representative model, useful for determining the principal controls on reservoir stress changes, and the directionality of stress changes introduced by varying material parameters. In this case, we suspect that the Young's modulus is overestimated by an unknown amount, and we know that reducing it will produce a stress path closer to that inferred from microseismic observations. This paper has demonstrated the importance of groundtruthing geomechanical models with geophysical observations from the field. To determine more exactly how much the Young's modulus needs to be reduced to get a good match with observation will probably require a more detailed model that provides a better match with the details of the reservoir geology, and a more precise way of determining how much of an increase in fracture potential is needed to generate microseismicity.

6. Conclusions

Monitoring of induced microseismicity has been conducted since 2003 in one pattern of the Weyburn CO_2 Storage and Monitoring Project. Event hypocenters indicate that most of the microseismicity is located around the nearby horizontal production wells, and not around the injection well as anticipated. Although the errors in vertical location are large, it appears that many events are located in the overburden. Observations of anisotropy made by measuring the splitting of S-waves also do not match with expectations based on core sample and borehole log work. Overall, the low rate of seismicity suggests either that there is little geomechanical deformation occurring, or that deformation is generally occurring aseismically.

In order to interpret these observations and understand what they mean for the risks of CO_2 leakage, it is necessary to construct geomechanical models of the injection process. For geomechanical models to be 'trusted', they must be matched with observations from the field. While there are many potential observables with which geomechanical models could be calibrated, the observations from Weyburn provide an opportunity to evaluate whether it is possible to match geomechanical models with observations of microseismicity.

We have generated a representative numerical geomechanical model of the Weyburn reservoir and surrounding units. This model couples together an industry standard fluid-flow simulator with a finite element mechanical solver. The initial model uses material properties based on core sample rock physics measurements, and does not do a good job of matching the microseismic observations. The most likely reason for this is that the stiffness of the reservoir has been overestimated. The presence of larger scale features such as fractures and vugs will not be accounted for in core sample analysis, and their effect will be to reduce the elastic stiffness of the unit, sometimes by quite a significant amount. By reducing the reservoir stiffness by an order of magnitude, we create a model that predicts that microseismic events will occur around the producing wells, and in the overburden above the producers. Although the reduction in stiffness we have made is perhaps overly large, our approach shows how geophysical observations in the field should be taken into account when developing geomechanical models.

Based on the inferences we have made from the geomechanical models, we propose that the events in the overburden are not caused by fluid migration into, or pore pressure changes in the overburden, but by stress transfer. S-wave splitting patterns generated by the softer model also match well with observation. The discrepancy between laboratory measured static stiffness and that needed to reproduce geophysical observations highlights the difficulties that can be encountered in upscaling laboratory measurements for use in field scale models.

This paper has presented a workflow that demonstrates how geomechanical models can be linked with observations of microseismicity, improving our interpretation of microseismic event locations and our confidence in our geomechanical models. It is important to calibrate and groundtruth any model of the subsurface, and microseismic observations, as a direct manifestation of mechanical deformation, can provide an important constraint for geomechanical models. The purpose of this paper is to demonstrate the concept. At present, the state of the art in geomechanical modelling, and in linking geomechanical models with geophysical observations, is probably not sufficiently advanced to fulfil the requirement that 'the conformity of the *actual* behaviour of the injected CO_2 with the *modelled* behaviour' (E.U. Parliament and Council, 2009) could be rigorously demonstrated in a manner analogous to reservoir modelling of CO_2 distribution and 4D seismic observations. Nevertheless, we anticipate that with more detailed and advanced geomechanical models, and a more rigorous method for predicting seismicity based on geomechanical models, further advances will be made.

7. Acknowledgements

The authors thank the PTRC and the Weyburn field operator, Cenovus, for making the microseismic data available. We are also grateful to the PTRC for funding. Shawn Maxwell and Marc Prince are thanked for their work on the microseismic hypocenters. Rockfield Software Ltd provided the geomechanical modelling software. This work was completed as part of the Bristol University Microseismicity ProjectS (BUMPS).

References

Angus, D.A., Kendall, J.M., Fisher, Q.J., Segura, J.M., Skachkov, S., Crook, A.J.L., Dutko, M., 2010. Modelling microseismicity of a producing reservoir from coupled fluid-flow and geomechanical simulation. Geophysical Prospecting 58, 901–914.

Angus, D.A., Verdon, J.P., Fisher, Q.J., Kendall, J.M., 2009. Exploring trends in microcrack properties of sedimentary rocks: An audit of dry core velocity-stress measurements. Geophysics 74, E193–E203.

Arts, R., Eiken, O., Chadwick, A., Zweigel, P., van der Meer, L., Zinszner, B., 2004. Monitoring of CO_2 injected at Sleipner using time-lapse seismic data. Energy 29, 1383–1392.

Bickle, M., Chadwick, A., Huppert, H.E., Hallworth, M., Lyle, S., 2007. Modelling carbon dioxide accumulation at sleipner: Implications for underground carbon storage. Earth and Planetary Science Letters 255, 164–176.

Brown, L.T., 2002. Integration of rock physics and reservoir simulation for the interpretation of time-lapse seismic data at Weyburn field, Saskatchewan. Master's thesis. Colorado School of Mines, Golden, Colorado.

Connolly, P.T., Cosgrove, J.W., 1999. Prediction of fracture induced permeability and fluid flow in the crust using experimental stress data. Bulletin of the AAPG 85, 757–777.

Dean, R.H., Gai, X., Stone, C.M., Minkoff, S.E., 2003. A comparison of techniques for coupling porous flow and geomechanics. Proceedings of the 17th SPE reservoir simulation symposium, SPE 79709.

Eckert, A., 2007. 3D multi-scale finite element analysis of the crustal state of stress in the Western US and the Eastern California Shear Zone, and implications for stress – fluid flow interactions for the Coso Geothermal Field. Ph.D. thesis. Universität Karlsruhe (TH).

E.U. Parliament and Council, 2009. Directive 2009/31/EC of the European Parliament and of the Council of 23 April 2009 on the geological storage of carbon dioxide. Official Journal of the European Union 52, L140/114.

Giese, R., Henninges, J., Lüth, S., Morozova, D., Schmidt-Hattenberger, C., Würdemann, H., Zimmer, M., Cosma, C., Juhlin, C., the CO2SINK Group, 2009. Monitoring at the CO2SINK site: A concept integrating geophysics, geochemistry and microbiology. Energy Procedia 1, 2251–2259.

Hatchell, P., Bourne, S., 2005. Rocks under strain: Strain-induced time-lapse time shifts are observed for depleting reservoirs. The Leading Edge 24, 1222–1225.

Hudson, J.A., Liu, E., Crampin, S., 1996. The mechanical properties of materials with interconnected cracks and pores. Geophysical Journal International 124, 105–112.

Jimenez, J.A., Chalaturnyk, R.J., Whittaker, S.G., Burrowes, G., 2004. A mechanical earth model for the Weyburn CO_2 Monitoring and Storage Project and its relevance to long-term performance assessment. Proceedings of the 7th International Conference on Greenhouse Gas Control Technologies.

Luo, M., Takahashi, I., Takanashi, M., Tamura, Y., 2005. Improved fracture network mapping through reducing overburden influence. The Leading Edge 24, 1094–1098.

Luo, M., Takanashi, M., Nakayama, K., Ezaka, T., 2007. Physical modeling of overburden effects. Geophysics 72, T37–T45.

Mathieson, A., Midgely, J., Dodds, K., Wright, I., Ringrose, P., Saoul, N., 2010. CO_2 sequestration monitoring and verification technologies applied at Krechba, Algeria. The Leading Edge 29, 216–222.

Maxwell, S.C., White, D.J., Fabriol, H., 2004. Passive seismic imaging of CO_2 sequestration at Weyburn. SEG Expanded Abstracts 23, 568–571.

Nur, A.M., Simmons, G., 1969. The effect of saturation on velocity in low porosity rocks. Earth and Planetary Science Letters 7, 183–193.

Onuma, T., Ohkawa, S., 2009. Detection of surface deformation related with CO_2 injection by DInSAR at In Salah, Algeria. Energy Procedia 1, 2177–2184.

Rutqvist, J., Vasco, D.W., Myer, L., 2009. Coupled reservoir-geomechanical analysis of CO_2 injection at In Salah, Algeria. Energy Procedia 1, 1847–1854.

Segura, J.M., Fisher, Q.J., Crook, A.J.L., Dutko, M., Yu, J., Skachkov, S., Angus, D.A., Verdon, J.P., Kendall, J.M., 2010. Reservoir stress path characterization and its implications for fluid-flow production simulations. *sub judice*, Petroleum Geosciences.

Shapiro, S.A., 2008. Microseismicity - a tool for reservoir characterization. EAGE Publications, NL.

Teanby, N.A., Kendall, J.M., van der Baan, M., 2004a. Automation of shear-wave splitting measurements using cluster analysis. Bulletin of the Seismological Society of America 94, 453–463.

Teanby, N.A., Kendall, J.M., Jones, R.H., Barkved, O., 2004b. Stress-induced temporal variations in seismic anisotropy observed in microseismic data. Geophysical Journal International 156, 459–466.

Verdon, J.P., Angus, D.A., Kendall, J.M., Hall, S.A., 2008a. The effects of microstructure and nonlinear stress on anisotropic seismic velocities. Geophysics 73, D41–D51.

Verdon, J.P., Angus, D.A., Kendall, J.M., Segura, J.M., Skachkov, S., Fisher, Q.J., 2008b. The effects of geomechanical deformation on seismic monitoring of CO_2 sequestration. SEG Expanded Abstracts 27, 2869–2873.

Verdon, J.P., Kendall, J.M., 2011. Detection of multiple fracture sets using observations of shear-wave splitting in microseismic data. *accepted*, Geophysical Prospecting.

Verdon, J.P., Kendall, J.M., Maxwell, S.C., 2010a. A comparison of passive seismic monitoring of fracture stimulation due to water versus CO_2 injection. Geophysics 75, MA1–MA7.

Verdon, J.P., Kendall, J.M., Wüstefeld, A., 2009. Imaging fractures and sedimentary fabrics using shear wave splitting measurements made on passive seismic data. Geophysical Journal International 179, 1245–1254.

Verdon, J.P., White, D.J., Kendall, J.M., Angus, D.A., Fisher, Q., Urbancic, T., 2010b. Passive seismic monitoring of carbon dioxide storage at Weyburn. The Leading Edge 29, 200–206.

White, D., 2009. Monitoring CO_2 storage during EOR at the Weyburn-Midale field. The Leading Edge 28, 838–842.

Zatsepin, S., Crampin, S., 1997. Modelling the compliance of crustal rock-I. Response of shear-wave splitting to differential stress. Geophysical Journal International 129, 477–494.

Zhou, R., Huang, L., Rutledge, J., 2010. Microseismic event location for monitoring CO_2 injection using double-difference tomography. The Leading Edge 29, 208–214.

Unit	*E (GPa)*	ν	ρ *(kg/m^3)*	ϕ	*Layer top (m)*	*Layer base (m)*
Overburden	5.0	0.25	2000	0.2	0	1210
Watrous	14.0	0.23	2000	0.1	1210	1410
Marly Evaporite	24.0	0.34	2700	0.05	1410	1430
Reservoir	14.5	0.31	2200	NA	1430	1470
Frobisher Evaporite	24.0	0.34	2700	0.05	1470	1490
Underburden	20.0	0.25	2500	0.1	1490	2490

Table 1: Material parameters for the units of the Weyburn geomechanical model. All layers are saturated with water with K=2.2GPa and ρ=1100kg/m^3, except the reservoir, whose porosity and fluid saturation are determined by the fluid-flow simulation.

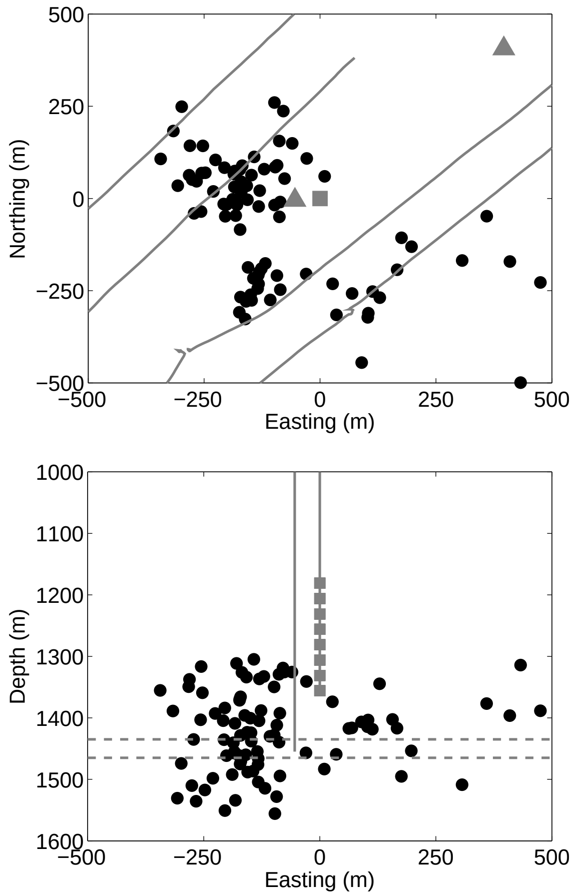

(a) (b)

Figure 1: Event locations in (a) map view and (b) cross section. The observation geophones are marked by squares, and the vertical injection wells are marked by the triangles in (a) and the left-hand vertical line in (b). The horizontal production wells are marked in (a), and the reservoir interval is marked by the dotted lines in (b). The majority of events are located closer to the production wells than the injection well, and many are located in the overburden.

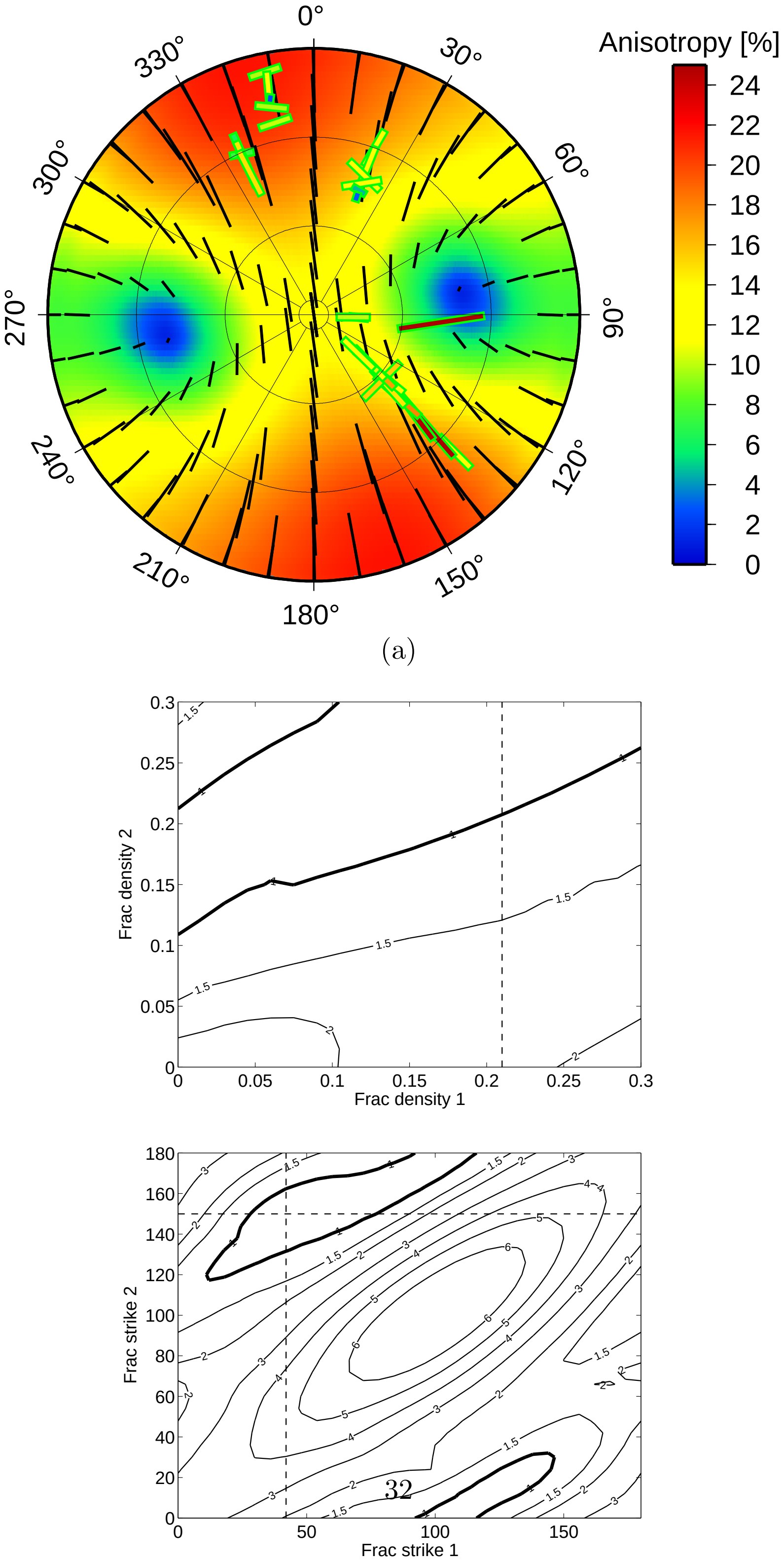

(a)

(b) (c)

Figure 2: Results of the inversion of SWS measurements for the densities and strikes of two vertical fracture sets. In (a) we show an upper hemisphere plot of the SWS measurements (coloured ticks) along with the results from the best-fit model (contours and black ticks). In (b) and (c) we plot the rms misfit surface as a function of fracture densities and of fracture strikes. (as per Verdon et al., 2009, 2010a; Verdon and Kendall, 2011). The

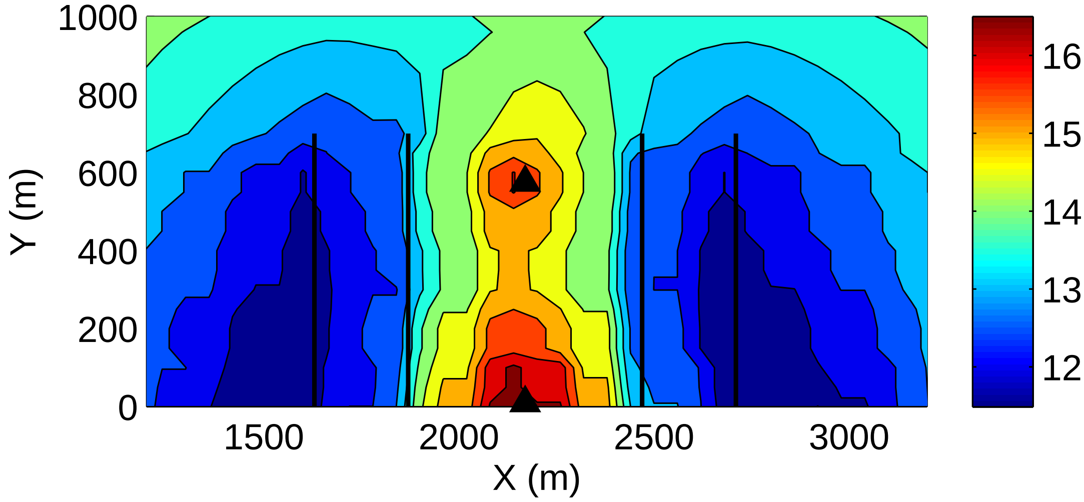

Figure 3: Map view of reservoir pore pressures (in MPa) after one year of injection computed by the fluid flow simulation of Weyburn. The vertical injection wells are marked by triangles, the horizontal producing wells by black lines. We have focused on the region of interest where production and injection occurs – the full model extends to $0 < x < 4400$m and $0 < y < 2000$m to include a 'buffer' area. Reflective symmetry along the x axis means that we can model only half the reservoir, and use symmetry arguments to complete the model.

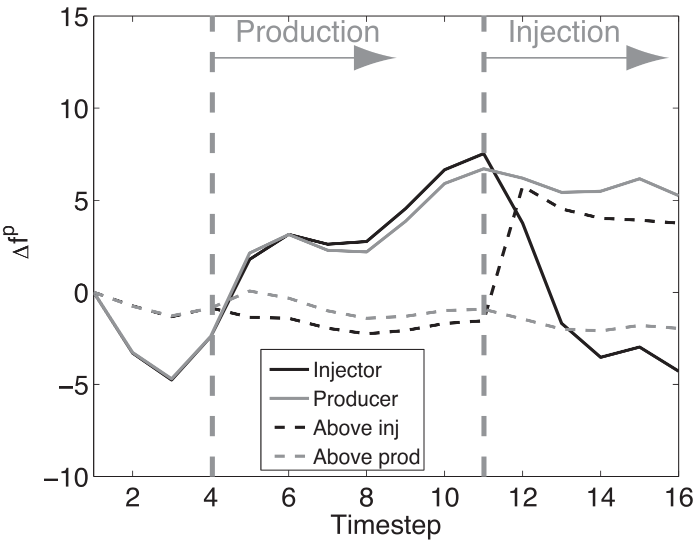

Figure 4: Percentage change in fracture potential in the Weyburn reservoir and overburden through time. f^ps in the reservoir injection well are marked by a solid lines, in the overburden by dashed lines. f^ps near the injection wells are marked in black, near the producers in gray. Fracture potential does not increase anywhere after injection begins (timestep 11) except in the overburden near the injection wells (black dashed line). Therefore this region should be most prone to microseismic activity.

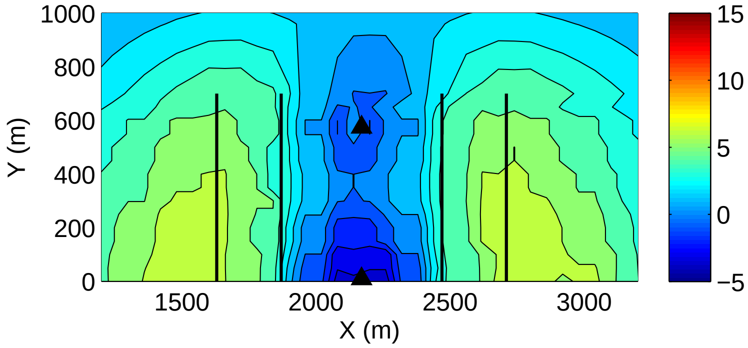

(a)

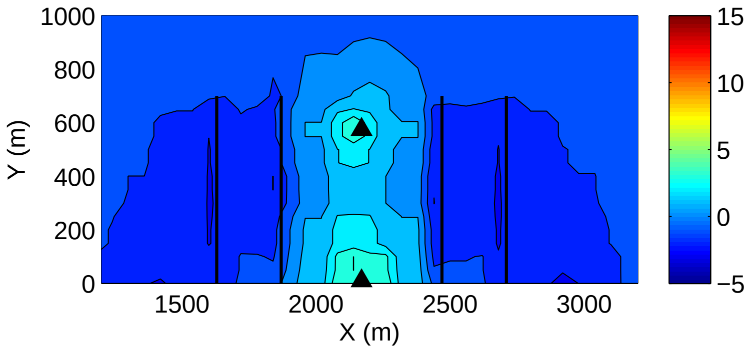

(b)

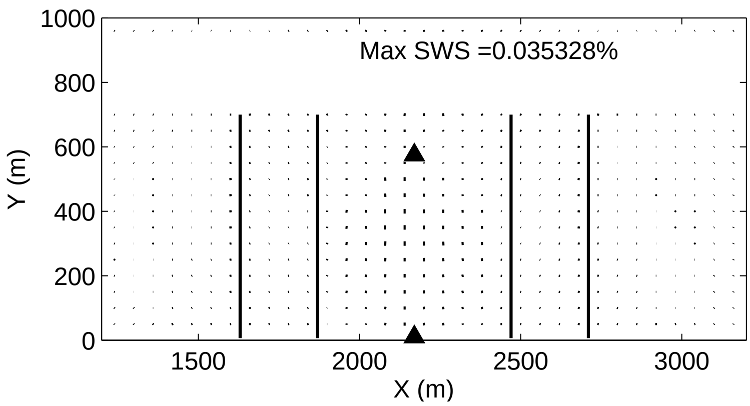

(c)

Figure 5: Map view of microseismic and SWS predictions from the geomechanical model of the Weyburn reservoir. The injection and production wells are marked as per Figure 3. In (a) and (b) we plot the percentage change from the initial state of fracture potential in the reservoir and overburden after injection. In the reservoir (a), fracture potentials are largest at the production wells. In the overburden (b), there is a small increase in the fracture potential above the injection wells. In (c) we plot the modelled splitting for a vertically propagating shear wave in the overburden. Tick orientations mark the fast direction, tick lengths mark the splitting magnitude, and the maximum splitting values are given. Little SWS has developed, implying little differential variation of the horizontal principal stresses.

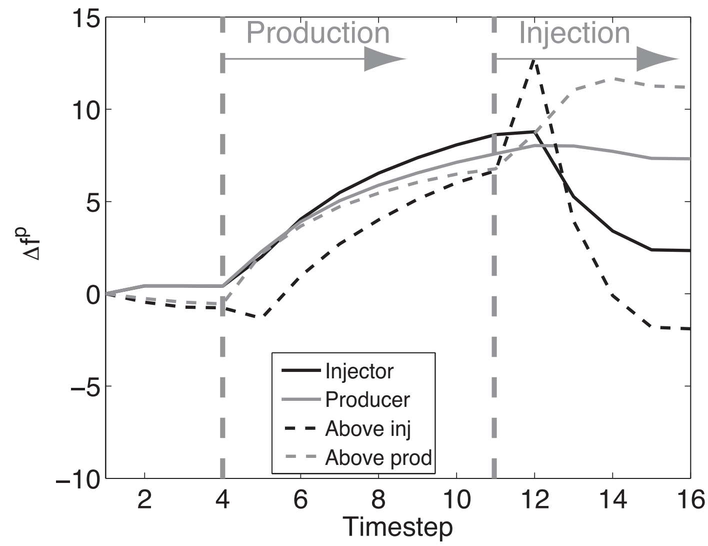

Figure 6: Percentage change in fracture potential in the softer Weyburn reservoir and overburden, as per Figure 4. After CO_2 injection begins (timestep 11), fracture potential is seen to increase in the overburden above the production wells (gray dashed line). After a transient increase, fracture potential above the injection well (black dashed line) decreases during injection.

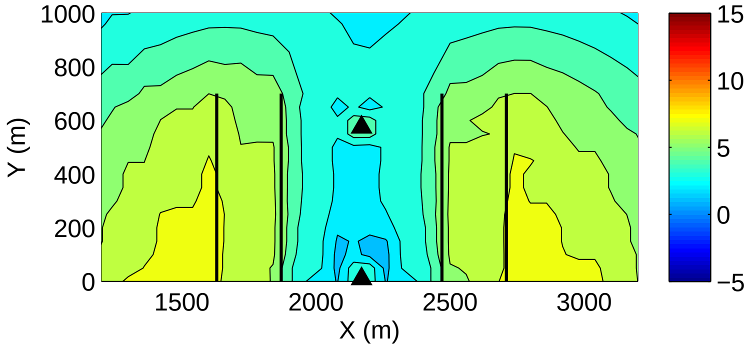

(a)

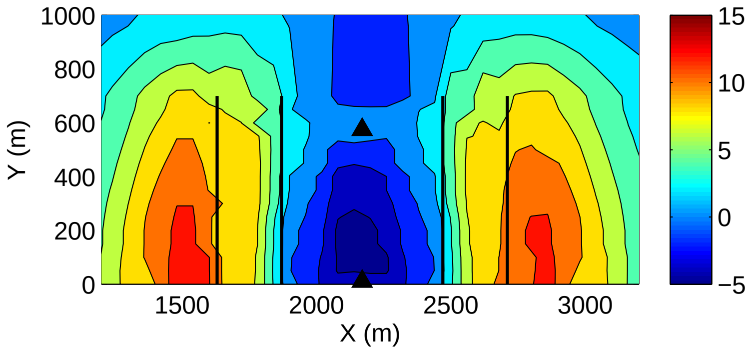

(b)

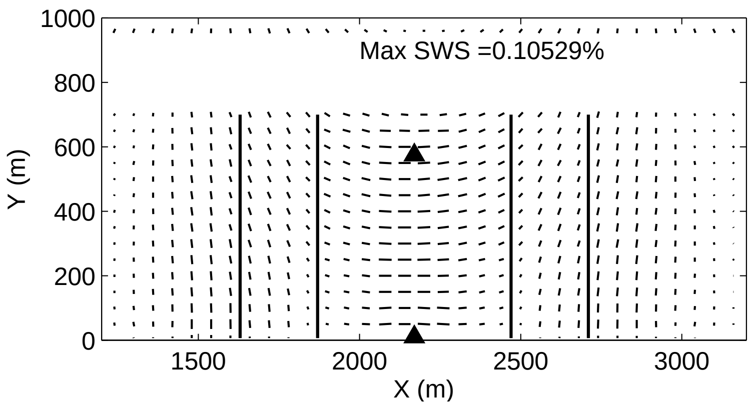

(c)

Figure 7: Microseismic and SWS prediction from the softer model of the Weyburn reservoir. In (a) and (b) we plot the fracture potential in the reservoir and overburden after injection. Fracture potentials increase at the production wells and in the overburden above the production wells. In (c) we plot the modelled splitting for a vertically propagating shear wave in the overburden. Anisotropy develops, causing SWS in the overburden, with the fast direction above the injection site perpendicular to the horizontal well trajectories.